GEOCHEMICAL SIGNATURE AND GEODYNAMIC SIGNIFICANCE OF AN Ag-Hg MINERALIZED DYKE SWARM IN THE NEOPROTEROZOIC INLIER OF IMITER - ANTI-ATLAS (MOROCCO)

Moha Ikenne*,✉, Aomar Ennaciri, Hassan Ouguir***, Brian Cousens°, Rachid Ziyadi°°, Mohamed Mouhagir**** and **Aziz El-Gaouzi****

* *LAGAGE, Département de Géologie, Faculté des Sciences B.P.8106, Agadir, Maroc.*
** *Société Métallurgique d'Imiter (SMI), MANGEM, Groupe ONA - Maroc.*
*** *Département de Géologie, Faculté des Sciences, Meknès. Maroc.*
° *Department of Earth Sciences, Carleton University, 1125 Colonel By Drive, Ottawa, Ontario, K1S5B6, Canada.*
°° *REMINEX, MANAGEM, Groupe ONA, Maroc.*
✉ *Corresponding author, email: moha_ikenne@yahoo.fr*

Keywords: *Dykes, silver deposits, extension, Late-Proterozoic. Imiter, Morocco.*

ABSTRACT

The Cryogynian basement of the Imiter Inlier and its volcanic cover are crosscut by an important swarm of mafic and felsic dykes. In the volcanic series, the dykes are oriented N-S to N70°E and emplaced within a E-W tensional stress field, whereas in the basement they are parallel to pre-existing planes ($S_0//S_1$) which vary in trend from N70°E to N90°E.

Silver mineralization is closely associated with mafic dykes that behaved as mechanical traps, either due to their brittle structural behaviour or by behaving as a barrier to fluid flow.

Two petrogenetic groups have been recognised in dyke rocks: the first group consists of basalts and basaltic-andesites, the second one corresponds to andesites, quartz-microdiorites, and keratophyres. Both groups are calc-alkalic and display geochemical features comparable to those of magmatic rocks from modern active continental margins and island arcs: large ion lithophile (LIL) element enrichments, high field strength (HFS) element depletion, and weakly fractionated rare earth element (REE) $(La/Yb)_N$ = 3.7 to 6.6) patterns.

Constraints of the regional geology suggest that these rocks were associated with post-orogenic, post-Panafrican rifting and preclude any subduction activity at that time. Their nature and their chemical signature can be related to: (i) the existence of fragments of an older subducted crust, (ii) partial melting of a mantle contaminated during the orogenic Panafrican stages or (iii) contamination during ascent of mantle derived magmas by African crust.

INTRODUCTION

During Late-Proterozoic times, the Anti-Atlas region was characterized by abundant calc-alkaline volcanism associated with an important dyke swarm. The significance of this post-collisional Panafrican magmatism is still controversial. Geochemical evidence is consistent with calc-alkalic volcanism related to subduction; however field geology and structural data are not consistent with this model (Bajja, 1987; Azizi et al., 1990; Zahour et al., 1999; Thomas et al., 2002).

Recent geochronological and geochemical data on the different economic mineral deposits of Imiter (Ag-Hg), Bou Madine (Zn-Cu-Pb-Sn-Ag-Au) and Bou Azzer (Co-Ni-As-Fe-Cu-Au-Ag) reveal that the Precambrian-Cambrian transition is an important period in the genesis of the majority of the deposits in the Anti-Atlas belt (Maacha et al., 1998; Baroudi et al., 1999; Cheilletz et al., 2002; Levresse et al., 2004; Gasquet et al., 2005). During this post-Panafrican period the Anti-Atlas has undergone a crustal thinning that caused hydrothermal fluid activity responsible for the formation of these deposits (Maacha et al., 1998; Levresse et al., 2004; Gasquet et al., 2005).

The aim of this study is to determine structural controls on the distribution of dykes and to clarify their potential role in the genesis of the main silver deposits. Preliminary data on petrology and geochemistry of dyke rocks possibly suggest a non-subduction geotectonic model to account for magmatism in this region.

GEOLOGICAL BACKGROUND

The Precambrian Anti-Atlas belt is tectonically divided into the south-western domain and the north-eastern domain by a major tectonic feature, the major fault of the Anti-Atlas (Fig. 1a). A striking contrast is noticed in the geological history between the southwest side and northeast side. Paleoproterozoic terrains and Eburnean tectonic events characterize the southwest side, whereas Neoproterozoic rocks are dominant in the northeast side.

On the basis of new geochronological data (Walsh et al., 2002; Gasquet et al., 2004; Thomas et al., 2004) a new lithostratigraphic framework is proposed for the Anti-Atlas (Fig.1b). It consists of an Eburnean basement unconformably overlain by a Neoproterozoic to Cambrian cover group. The cratonic basement consists of a silicoclastic Paleoproterozoic series intruded by granitoids dated at 2050-1760 Ma. It is represented by the Zenaga, Kerdous and Drâa Complexes in the Sirwa, Kerdous and Bas Drâa Inliers, respectively. The Neoproterozoic cover group is divided into two lithostratigraphic units: (1) the Anti-Atlas supergroup, including Cryogenian to early Ediacarian rocks of the Bleida, Saghro Groups and their equivalent in the western Anti-Atlas. These groups are attributed to a passive margin, oceanic and island-arc stages of the Panafrican events and are associated with igneous rocks dated at 661±23 to 762±2 Ma (Gasquet et al., 2005); (2) The Ouarzazate Supergroup, a late syn- to post-tectonic, continental volcanic and clastic sequence, associated with high-K calc-alkaline to shoshonitic and alkaline magmatism dated at 600 ± 5 to 531 ± 5 Ma (Thomas et al., 2004). The transition to the Paleozoic series (Tata Group) is exemplified by the transgressive series of the Taroudante Group, associated with trachytic sills and the Jbel Boho syenite dated respectively at 531 ± 5 and 529 ± 3 Ma (Ducrot et Lancelot, 1977; Gasquet et al., 2005).

Two tectonic events have been recognized in the Panafrican belt of the Anti-Atlas (Leblanc, 1981; Hassenforder, 1987; Saquaque et al., 1989). The first one, the major Panafrican stage (B1) dated at 685 ± 15 Ma, affects the Bleida Group series and produced recumbent isoclinal folds verging towards WSW associated with a metamorphic schistosity. The second event (B2) is called the late Panafrican stage, affecting the Bleida as well as the Saghro Group series, and is dated at 615 ± 12 Ma. It has produced upright folds with N115 subhorizontal axes accompanied by cleavage without metamorphic recrystallization. However, recent studies in the western Anti-Atlas (Soulaimani et al., 2003; Soulaimani and Piqué, 2004; Oudra et al., 2005) report that there is no evidence of fold structures related to the B2 compressive phase.

The Imiter Inlier, famous for its silver deposits, is located at the northern part of the Saghro Massif in the Panafrican domains. According to Ouguir et al. (1994) and Baroudi et al. (1999), it consists of a Cryogynian basement and a late Neoproterozoic cover (Fig. 1c). The Cryogynian basement is made up of black shales and greywackes deposited at the bottom of a continental slope (Marini and Ouguir, 1990; Ouguir et al., 1994). The cover group consists of a thick volcanic and volcaniclastic series (conglomerates, andesites, rhyolite lavas and pyroclastics). The Cryogenian series is affected by two compressive events. The first, related to the B1 phase, produced hectometric to decametric folds. The associated axial plane cleavage turns from NE-SW in the southwestern part of the basement to E-W in the northwestern part (Ouguir et al., 1994). The second event is responsible for N110°E-trending folds that are not associated with any cleavage. This second event corresponds to the late Panafrican compressive phase (B2).

The structural analysis of the fault framework in the volcaniclastic cover is consistent with a succession of 3 main tectonic regimes: (1) an extensional NNW-SSE stress regime evolving to (2) a normal-sinistral movement due to more oblique extension (NW-SE) and (3) the most recent ~ ENE-WSW extension, recorded by N120-150°E faults showing normal movement.

FIELD RELATIONS AND PETROGRAPHY OF DYKE ROCKS

Dykes intrude the Cryogynian basement and its late Neoproterozoic volcanic cover with widths ranging from 50 cm to 3 m. The dykes and their host rocks are unconformably overlain by the Palaeozoic (Middle Cambrian) series. The map and rose diagram of dykes (Fig. 1c and 2a) show a

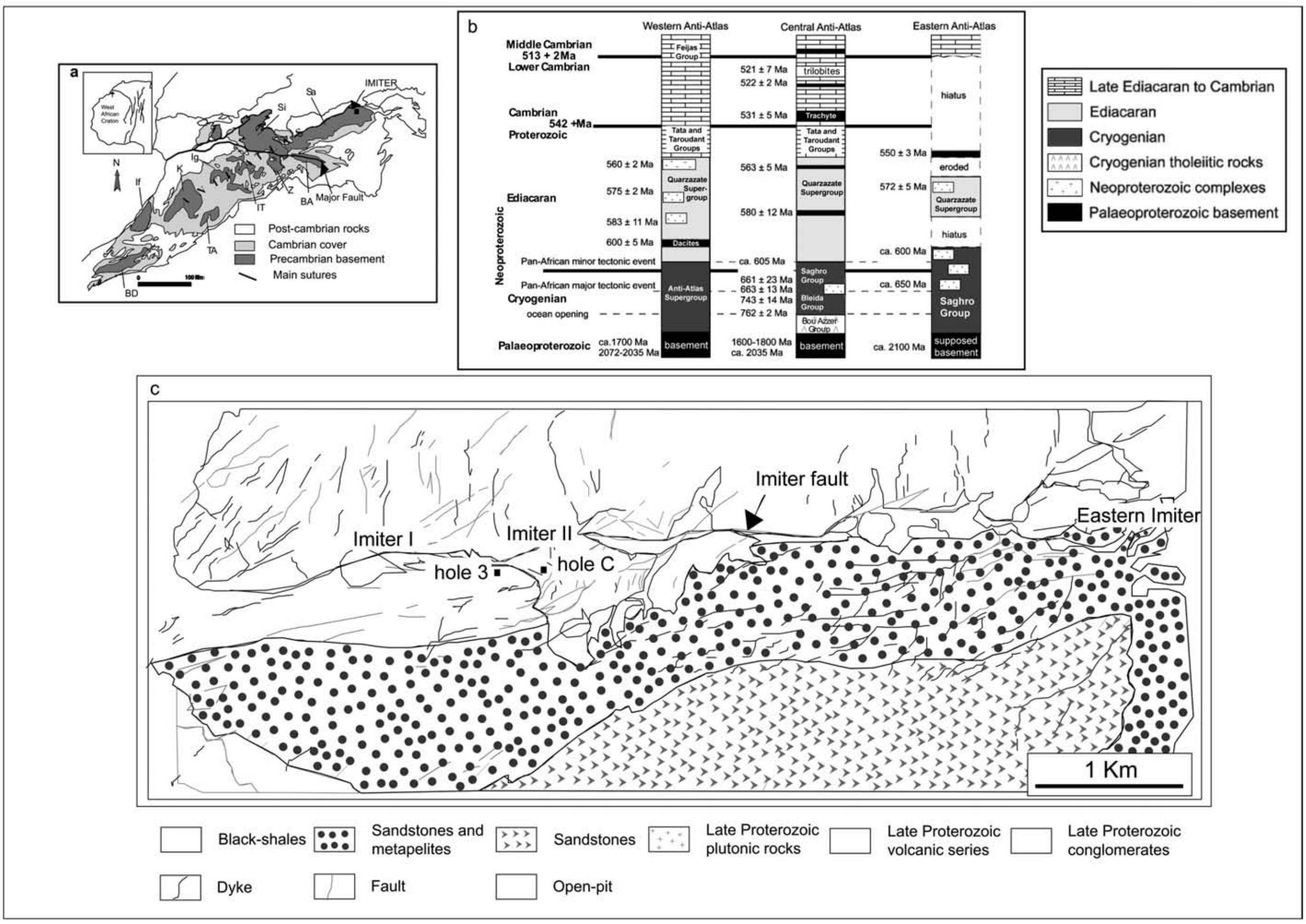

Fig. 1 - (a) The Proterozoic inliers of the Anti-Atlas and location of the Imiter Inlier. BD- Bas Drâa; If- Ifni; K- Kerdous; Ig- Ighrem; TA- Tagragra d'Akka; IT- Iguerda-Taifast; S-: Sirwa; BA- Bouazzer; Z- Zenaga; Sa- Saghro. (b) Timetable of the Proterozoic events in the Anti-Atlas belt, from Gasquet et al. (2005). (c) Geological map of the Imiter Inlier (from the Geological Survey of the Imiter Mine company: SMI).

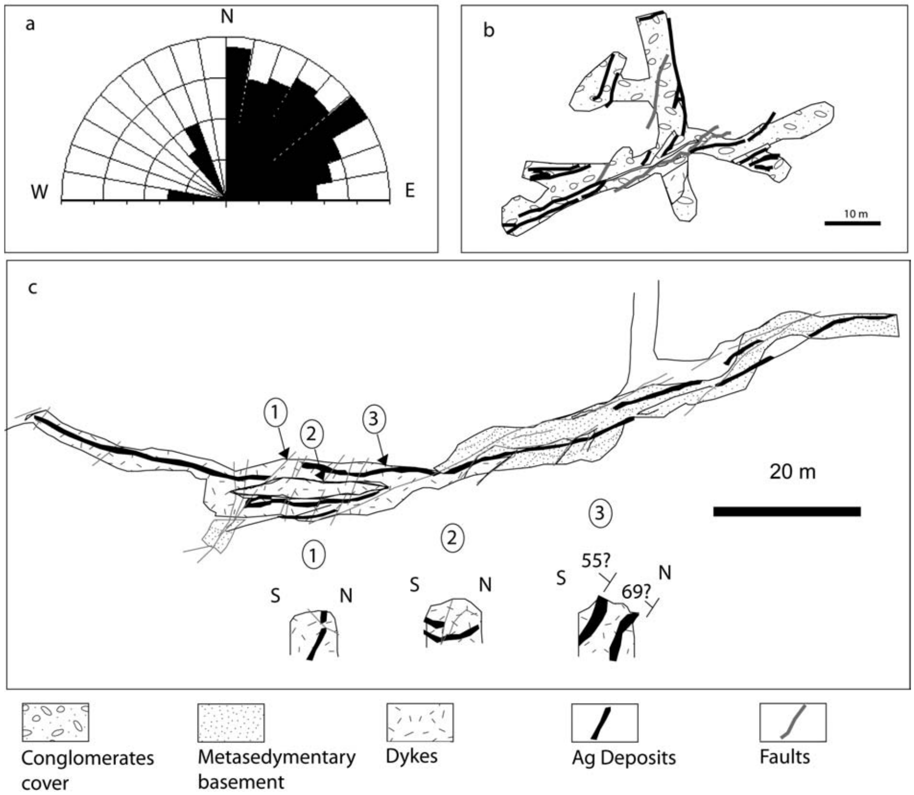

Fig. 2 - Maps of the underground mine showing the relationships between silver mineralization and dykes: a- Rose diagram for late Proterozoic dykes of the Imiter Inlier (realized from the aerial photographs at 1/8000); b- In the late Proterozoic cover; c- In the Gryogenian basement.

wide variety of orientations, from N-S to N 70°E, although the dominant trends are N 00-10°E and N60-70°E. Some N 70°E oriented dykes seem to be emplaced along an "en echelons" system. The dykes cross-cut bedding, S1 and S2 foliations, but they can also be concordant with S1 mainly in the central basement part of the inlier. The dykes are actually parallel or sub-parallel to the pre-existing structures, suggesting that the dykes were emplaced into zones of weakness that originated as fractures or schistosity planes. The sub-meridian dykes, more abundant in the volcano-detrital cover, are affected by tectonic deformation related to the Imiter fault.

Dyke rocks are classified into three categories based on petrography mineralogy and texture: (1) basalts and basaltic andesites, (2) andesites, and (3) felsic rocks. The basalts and the basaltic andesites are fine grained with microlitic or glassy texture. Most of the samples are plagioclase-phyric with phenocrysts (2 - 3 mm) of olivine and amphibole, respectively, transformed into serpentine and calcite (± chlorite). The groundmass consists dominantly of microlites of plagioclase and a completely devitrified glass now composed of chlorite and very fine grained oxides. Fissures and vesicles are predominantly filled with calcite. The andesites differ from basalts in their small amount of ferromagnesian minerals and the appearance of quartz microcrystals. The acidic rock group comprises micro-quartz diorite, keratophyres and dacites. The quartz-microdiorites can be described as dolerite in outcrop because of their doleritic texture; their primary mineralogy consists of plagioclase, amphibole and interstitial quartz. The plagioclase is often altered to sericite and the amphibole completely pseudomorphed by a calcite-titanite assemblage. The differentiated central part of the dykes displays granophyric texture and includes the least amount of amphibole. The keratophyres and dacites are aphyric to sparsely phyric, with plagioclase phenocrysts in a microlitic groundmass. The dacites are commonly spherulitic and contain a significant amount of quartz.

ECONOMIC MINERALIZATION

The Imiter Ag-Hg deposit is hosted in Crygenian black shales and in the late Neoproterozoic volcaniclastic cover group. The mineralization is attributed to the NNW-SSE extensional tectonic stage which produced hydraulic fracturing of the black shales and the lower volcaniclastic series along the Imter fault zone (Ouguir et al., 1994). From the metal-rich black shales**,** two main stages of silver deposition have been recognized (Baroudi et al., 1999; Levresse et al., 2004): (1) a hydrothermal base metal event, with quartz (Qtz_1) as the gangue phase, associated with calc-alkaline magmatism at 572 Ma, and (2) an epithermal event responsible for the giant deposit associated with the felsic volcanic rocks dated at ca. 550 Ma (U-Pb on zircon; Levresse, 2001). This epithermal event occurred in two stages with quartz (Qtz_2) and dolomite as gangue phases, respectively (Baroudi et al., 1999). The first stage was characterized by hot fluids [Th (homogeneisation temperature) = 100-450°C and Tmi (melting temperature of ice) = -19-0.1°C]), whereas the second stage was cooler (Th = 115- 192°C and Tmi = -27.2 - -18°C). Guillou et al. (1988) suggested a supergene secondary origin for the silver and fluids. Boroudi et al. (1999) proposed a model with two different epithermal fluids for deposition of the silver: a cool and basinal fluid dissolved and leached the silver from the black shales, and the precipitation of silver occurred when this fluid was mixed with a hot magmatic fluid. However, investigations on sulphur, helium, and osmium isotopes and the compositions of fluid inclusions in sulphide phases and gangue minerals associated with the silver mineralization (Levresse et al., 2004) argue for a mantle origin of the metals and for a very limited contribution from the black shale reservoir.

Detailed mapping, carried out in the Cryogenian basement as well as in the upper Proterozoic cover, reveals that the ore body silver mineralization is closely associated with mafic dykes. Fractures along or cutting dykes contain large deposits of native plate silver weighing more than 100 kg.

In Hole "C" of the Imiter II deposit (Fig. 2b), the drift is a crosscut in the Upper Proterozoic series. At the 1436 m level, the gallery is about 4m in width and has a ENE-WSW trend in the "conglomérat de base" of the basement but a N-S trend in the pyroclastic rocks of the cover series. N15 to N45°E oriented felsic dykes cut this series. The silver deposits are located along the contact between dykes and host rock with an E-W to WSW-ENE trend. The gangue minerals consist mainly of quartz and dolomite**.** Away from the competent dykes, the mineralized lodes rapidly decrease in thickness and the mineralization becomes more diffuse and eventually disappears.

In Hole "3" main body of Imiter II, the drift crosscuts the Crygenian black shales of the basement. At the 1350 m

Table 1 - Major-element analyses of Imiter dyke rocks.

	basalts						basaltic andesites			micro-quartz diorites			Andesites				Keratophyres		
sample	IM 3	IM 16	IM 15	IM 30	IM 37	IM 34	IM 36	IM 2-19	IM 2-22	IM 4	IM 26	IM 33	IM 8	IM 14	IM 18	IM 2-24	IM 39	IM 49	IM 2-15
SiO_2	50,71	48,6	52,61	51,99	46,26	47,51	44,9	50,61	50,92	63,19	59,84	64,62	62,59	54,9	62,64	62,09	64,68	62,27	63,08
TiO_2	1,1	0,99	1,13	0,85	0,86	0,79	0,78	0,74	1,1	0,66	1,14	0,7	0,67	0,97	0,69	0,62	0,71	0,65	0,71
Al_2O_3	15,5	14,68	15,78	15,64	15,97	15,74	13,88	16,41	15,62	14,81	15,52	15,32	15,04	18,22	15,24	13,49	15,49	14,8	14,91
Fe_2O_3T	8,18	8,76	7,59	10,34	10,75	8,37	8,92	8,15	8,32	5,24	6,71	6,19	5,34	6,15	5,83	3,84	2,84	5,61	5,05
MnO	0,16	0,28	0,17	0,18	0,23	0,18	0,22	0,21	0,14	0,13	0,16	0,11	0,13	0,1	0,11	0,17	0,11	0,13	0,11
MgO	6,89	8,95	6,13	7,38	6,2	3,77	4,31	5,13	6,68	1,8	2,68	1,03	1,85	2,84	1,65	2,36	1,11	1,92	1,74
CaO	3,06	4	2,35	1,64	3,08	8,9	10,76	3	2,79	1,62	1,9	0,45	1,64	2,19	1,2	3,06	1,49	1,78	1,6
Na_2O	2,61	1,08	1,23	0,1	0,05	0,76	0,46	0,08	2,29	3,73	3,88	3,81	4,14	3,21	4,11	4,36	4,31	3,95	3,46
K_2O	3,39	2,76	5,95	4,24	8	3,36	2,72	6,58	4,02	4,82	4,45	4,74	4,61	5,45	4,23	2,83	4,36	4,7	5,3
P_2O_5	0,34	0,27	0,33	0,23	0,14	0,18	0,19	0,22	0,34	0,23	0,46	0,24	0,25	0,25	0,24	0,21	0,24	0,22	0,25
LOI	7,91	9,57	7,11	7,34	8,93	10,81	13,34	8,89	7,67	3,82	3,33	2,88	3,7	5,6	4,11	6,91	4,7	4,12	3,79
Total	99,85	99,94	100,38	99,93	100,47	100,37	100,48	100,02	99,89	100,05	100,07	100,09	99,96	99,88	100,05	99,94	100,04	100,15	100

Table 2 - Trace element analyses and selected discriminant trace element ratios of dyke rocks from Imiter Inlier.

	basalts						basaltic andesites			micro-quartz diorites			Andesite				Keratophyres		
sample	IM 3	IM 16	IM 15	IM 30	IM 37	IM 34	IM 36	IM 2-19	IM 2-22	IM 4	IM 26	IM 33	IM 8	IM 14	IM 18	IM 2-24	IM 39	IM 49	IM 2-15
As	68,15	43,17	63,03	155,00	32,57	9,94	30,65	55,26	144,80	7,27	8,74	56,97	5,83	38,44	10,47	104,80	11,00	32,62	7,72
Ba	424,60	922,10	1660,00	1025,00	1303,00	483,70	341,00	2122,00	644,20	2053,00	2486,00	2237,00	2119,00	789,50	2043,00	987,90	1982,00	2441,00	1572,00
Be	bd	1,59	bd	1,91	bd	1,93	bd	1,84	bd	bd	bd	bd	bd	1,91	bd	bd	bd	bd	bd
Ce	37,08	33,64	33,61	33,12	23,73	31,94	43,14	39,84	35,03	74,88	81,51	72,51	79,61	30,75	69,84	56,77	59,65	66,33	75,56
Co	35,30	41,51	39,81	43,38	26,24	23,57	38,44	40,29	32,27	31,90	23,38	23,54	27,02	34,04	29,18	43,56	44,34	22,52	45,53
Cr	167,00	415,90	309,70	716,10	87,31	60,98	290,90	232,80	207,90	9,19	5,14	9,85	bd	8,63	9,85	59,53	6,75	bd	25,62
Cs	2,97	4,82	1,23	4,48	2,07	6,48	5,17	6,16	2,74	0,86	0,95	1,84	0,90	4,62	1,15	0,43	0,81	0,87	0,82
Cu	13,98	18,84	12,86	21,47	13,07	26,32	52,95	6,88	17,12	bd	5,03	7,82	bd	36,85	bd	5,20	bd	9,03	bd
Dy	4,08	3,25	3,48	2,69	2,55	2,92	3,11	4,28	3,77	5,85	5,97	5,50	5,77	3,25	5,59	5,69	5,99	5,96	5,67
Er	2,31	1,79	2,10	1,64	1,56	1,69	1,60	2,86	2,18	3,52	3,08	3,26	3,21	1,86	3,17	3,33	3,67	3,29	3,24
Eu	1,09	1,29	1,00	0,65	0,84	1,02	1,41	0,93	1,15	3,48	5,25	3,36	4,83	0,77	3,88	3,53	4,27	3,90	4,81
Ga	18,29	16,36	17,59	17,20	17,69	18,60	16,09	15,86	18,03	19,35	20,28	19,88	19,08	19,90	21,32	16,86	19,77	20,20	18,32
Gd	4,29	3,86	3,81	3,13	2,97	3,25	4,04	4,58	4,20	6,94	7,95	5,87	7,01	3,78	6,34	6,42	6,50	7,34	6,67
Ge	1,06	1,13	1,14	1,44	1,28	1,84	1,80	1,30	1,25	1,16	0,96	1,18	1,08	1,16	1,38	0,83	0,93	0,98	1,16
Hf	3,25	2,74	3,33	2,24	2,32	2,58	1,96	2,35	3,22	12,35	6,71	11,69	12,20	3,59	12,48	10,51	12,96	12,15	12,23
Ho	0,80	0,64	0,72	0,54	0,52	0,59	0,59	0,92	0,75	1,21	1,17	1,13	1,14	0,67	1,12	1,17	1,24	1,15	1,11
La	15,19	14,72	14,27	16,18	11,32	14,63	20,44	17,37	15,71	31,58	40,37	27,15	32,18	12,97	31,55	26,93	28,10	30,31	32,95
Lu	0,31	0,26	0,32	0,28	0,28	0,26	0,24	0,49	0,29	0,56	0,49	0,56	0,53	0,28	0,56	0,51	0,61	0,52	0,56
Mo	1,51	0,96	2,73	1,14	0,97	bd	0,48	1,57	1,97	5,00	1,64	1,46	2,95	6,06	4,67	5,29	3,26	1,97	5,18
Nb	4,80	3,79	4,76	3,48	2,37	4,30	2,65	2,54	5,29	9,53	9,18	10,44	9,42	6,22	10,51	9,66	10,84	10,12	10,61
Nd	21,77	19,72	19,14	17,46	13,76	18,51	24,92	23,87	20,54	38,32	43,15	32,72	39,60	17,88	36,32	31,13	33,42	35,35	38,17
Ni	30,69	64,16	60,22	100,90	17,30	12,36	59,72	25,10	35,55	bd	bd	9,61	bd	9,28	bd	10,97	9,02	bd	bd
Pb	87,29	31,93	24,08	239,19	44,07	3,44	8,69	61,86	55,40	55,99	31,16	148,60	119,59	9,33	58,50	154,42	96,14	268,93	18,66
Pr	5,05	4,68	4,58	4,39	3,25	4,31	5,98	5,63	4,86	9,42	10,09	7,97	9,93	4,31	8,79	7,69	7,93	8,91	9,17
Rb	83,79	83,16	122,60	143,00	154,60	188,10	150,20	222,90	81,86	97,11	106,60	97,39	102,00	171,50	83,78	52,85	92,47	105,80	86,43
Sb	7,09	3,67	2,46	4,51	2,41	4,80	3,71	4,97	5,77	1,75	1,26	2,38	1,75	3,74	1,90	2,07	1,68	3,69	1,64
Sm	4,77	4,29	4,21	3,69	3,30	3,86	5,28	4,96	4,46	8,00	8,97	6,74	8,12	3,95	7,30	7,12	7,17	7,90	7,82
Sn	0,90	0,68	1,47	4,27	0,87	1,02	0,71	0,78	1,17	1,87	1,49	1,55	1,90	1,25	1,70	1,55	1,89	1,74	2,04
Sr	72,21	136,20	87,57	40,44	67,13	174,00	267,00	61,91	110,50	105,20	102,80	79,66	107,90	78,57	136,50	87,27	135,10	124,20	93,08
Ta	0,54	0,44	0,51	0,31	0,23	0,38	0,24	0,28	0,48	1,33	1,07	1,11	1,32	0,90	1,24	1,39	1,59	1,22	1,54
Tb	0,66	0,55	0,58	0,47	0,44	0,49	0,56	0,68	0,64	1,01	1,11	0,91	1,01	0,54	0,94	0,97	1,03	1,05	0,98
Th	2,18	1,84	2,24	4,63	1,45	2,54	4,34	2,51	2,29	6,49	5,75	6,90	6,48	3,39	7,18	6,31	7,51	7,24	7,24
Tm	0,32	0,25	0,30	0,25	0,25	0,24	0,21	0,43	0,30	0,52	0,45	0,51	0,48	0,27	0,47	0,47	0,55	0,49	0,48
U	1,28	1,06	2,20	3,56	1,53	1,36	2,83	3,79	1,57	4,40	3,57	4,44	4,36	1,31	5,27	5,12	6,07	4,57	5,37
V	167,70	169,90	179,10	222,00	187,30	188,50	201,60	228,20	173,60	6,27	43,54	8,89	6,83	92,34	6,78	8,62	6,81	6,77	6,04
W	88,85	57,51	68,24	33,69	20,05	38,51	31,92	47,34	39,67	312,30	179,40	175,80	315,50	240,60	229,40	387,70	381,10	219,70	380,50
Y	23,84	18,17	21,16	17,36	15,36	16,42	16,76	27,71	21,72	35,89	35,90	35,57	34,78	18,92	33,19	36,86	37,80	34,77	33,49
Yb	2,11	1,69	2,02	1,69	1,74	1,67	1,55	3,10	1,96	3,47	3,00	3,50	3,26	1,76	3,38	3,15	3,75	3,30	3,36
Zn	122,90	99,15	104,80	234,60	152,90	114,30	125,80	71,97	253,40	111,90	55,35	498,30	91,44	121,20	49,75	67,60	44,88	679,80	65,60
Zr	116,90	94,13	120,30	82,99	89,36	92,35	68,77	83,59	125,20	647,30	312,80	639,40	641,40	120,80	654,10	564,90	674,70	651,40	653,10
Zr/Nb	24,3796	24,8495	25,28905	23,8477	37,70464	21,47674	25,9705	32,8577	23,6628	67,90098	34,0815	61,2452	68,11086	19,4119	62,236	58,4843	62,2417	64,3676	61,5551
Zr/Yb	55,4554	55,8304	59,70223	48,99055	51,38585	55,43217	44,3391	26,98192	63,845	186,6494	104,4059	182,529	196,5676	68,7536	193,463	179,22	179,968	197,215	194,607
Nb/Y	0,20	0,21	0,22	0,20	0,15	0,26	0,16	0,09	0,24	0,27	0,26	0,29	0,27	0,33	0,32	0,26	0,29	0,29	0,32

bd = below detection limit.

level, the gallery trends E-W (Fig. 2c). The meta-sedimentary series shows a S0 //S1 oriented N60-75°E, N60-75° WNW. An E-W trending, 5 m thick mafic dyke cuts the black shales. The main Ag deposits consist of infillings of fractures contained within the dyke. These fractures are parallel to the dyke margins and are 20 cm thick. The silver is associated with a gangue mineral group of quartz, dolomite, limonite and galena. The mineralized veins are affected by sub-meridian fractures that can develop 1 m displacement.

We infer that the dykes behaved as mechanical traps for the silver mineralization, either due to their brittle structural behaviour or by behaving as barriers to fluid flow.

CHEMICAL COMPOSITION AND GEOCHEMICAL SIGNATURE OF THE DYKES

Twenty whole-rock samples of the dykes were analyzed for major, trace and rare earth elements. The analyses were carried out by ICP-AES for major elements and ICP-MS for trace and rare earth elements at the CRPG Nancy (France). Major and trace element data are presented in Tables 1 and 2.

The secondary assemblage of the Imiter dyke rocks is dominated by carbonate, chlorite and iron oxide minerals, occurring as vesicles and vein filling, and replacement of groundmass and primary minerals. The high degree of alteration is reflected in loss-on-ignition (LOI) values that range from 2.9 to 13.3 wt%. A very marked correlation between LOI and SiO_2, Na_2O, CaO, MgO is observed (Fig. 3). SiO_2 and Na_2O were leached during alteration. In contrast, TiO_2, Al_2O_3, P_2O_5 and paradoxically K_2O seem not to be affected by the alteration process.

Geochemically, the Imiter dykes form a continuum in composition with a wide range in SiO_2 (50.53-76.84 wt%), CaO (0.46-4.42 wt.%), Fe_2O_3t (2.97-9.69), MgO (1.05-9.90), K_2O (3.04-8.73) and Na_2O (2.97-9.69). Plotted against MgO (Fig. 4), the major elements show significant trends broadly compatible with crystal fractionation of observed phases, including plagioclase, olivine and clinopyroxene. Al_2O_3 is roughly constant, with high content (> 16 wt%) in the basic group and 14.4 to 19 wt% in the interme-

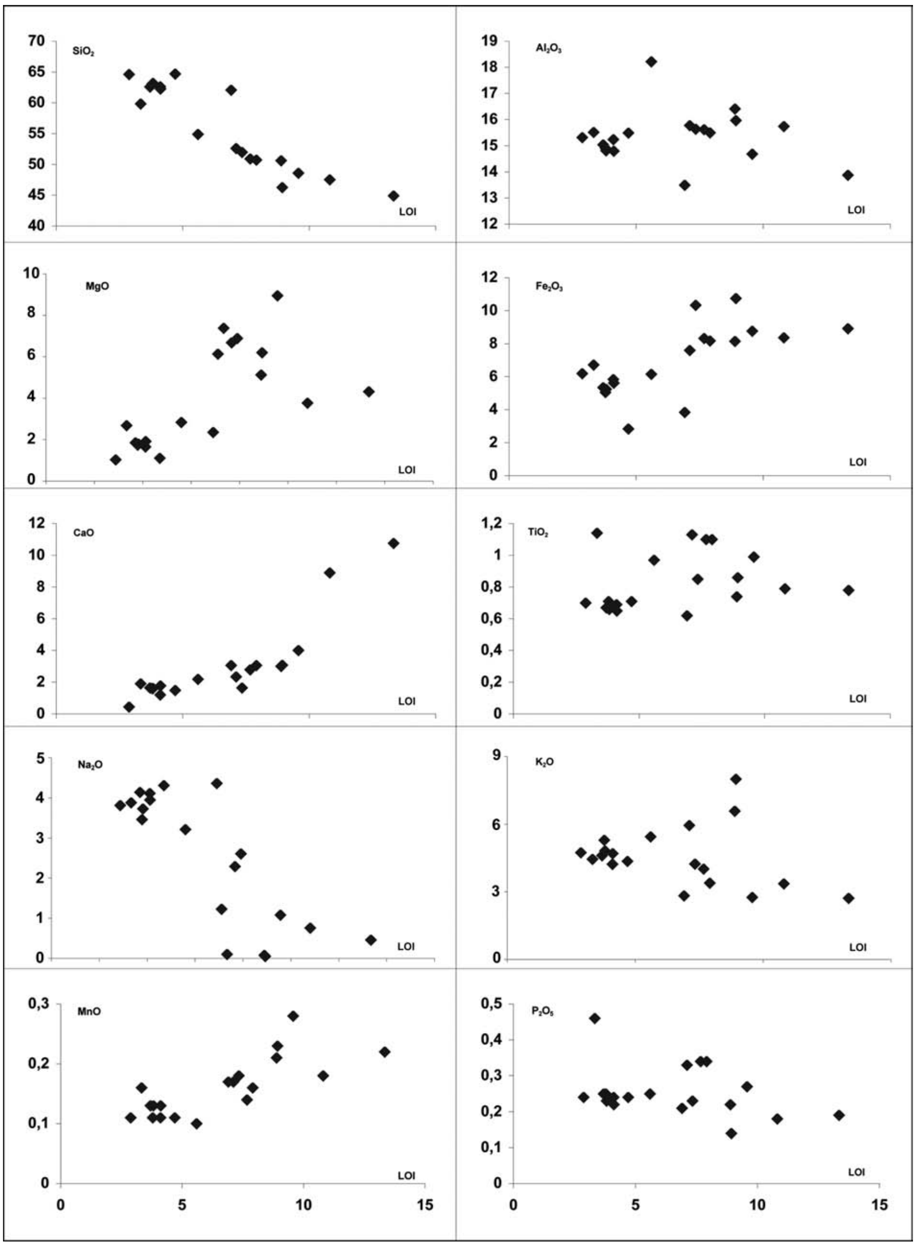

Fig. 3 - Major element compositions plotted against LOI.

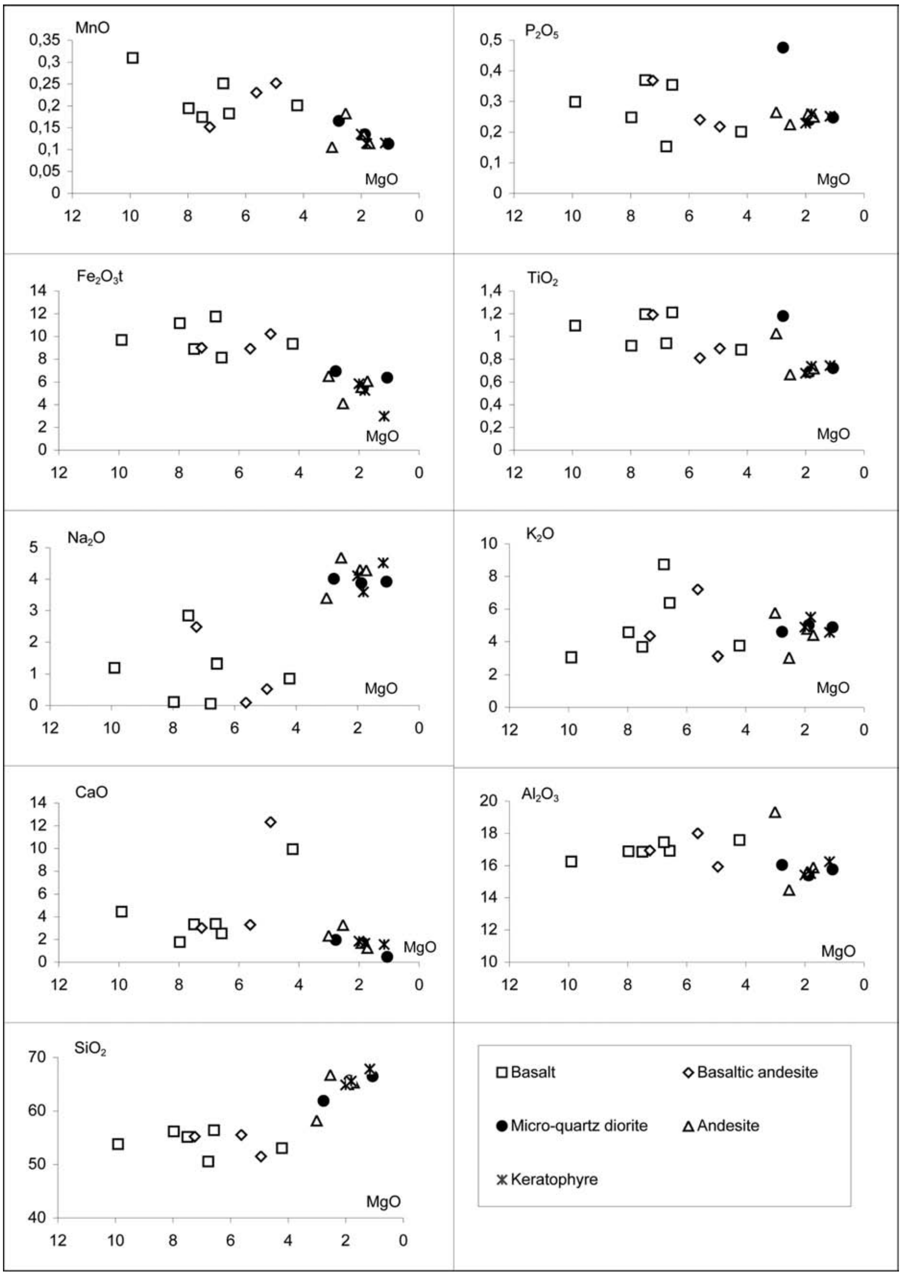

Fig. 4 - Major element variation diagrams against MgO (all in wt%, recalculated analyses without loss on ignition).

diate and felsic rocks. TiO_2 and Fe_2O_3t decrease markedly from basalts to keratophyres.

Trace elements are more discriminant among the Imiter dyke rocks, although the high degree of alteration must be taken into consideration (e.g., the LILE are highly mobile). The dyke types can be distinguished using immobile trace element ratios, particularly Zr/Yb, Zr/Nb and Nb/Y (Fig. 5 and Table 2). They are high in intermediate and felsic rocks (respectively > 104, > 60 and ≥ 0.26) and relatively low in the mafic rocks (respectively < 64, < 38 and ≥ 0.22).

Rare earth element Chondrite-normalized patterns are roughly parallel with $(La/Yb)_N$ ratio ranging from 4.39 to 8.89 (Fig. 6). The evolved rocks are distinguished by higher REE contents, with ΣREE ranging from 154 to 212 ppm, and a strong positive Eu anomaly (Eu/Eu* = 1.56). The basaltic andesite number IM 2-19 shows an unusual HREE enriched profile ($(La/Yb)_N$ = 3.78) and low Zr/Nb ratio. However, the mafic rocks have low REE contents (ΣREE = 66 - 113 ppm) and a negative Eu anomaly (Eu/Eu* = 0.60-0.83).

The higher Zr/Yb, Zr/Nb and Nb/Y ratios in the differentiated rock relative to the mafic rocks, and the observed gaps in REE and the HFSE contents, argue against a direct genetic relationship between the two rock groups. Instead, they are inferred to have derived from different parent magmas.

MORB normalized incompatible element variation diagrams are shown in Fig. 7. The mafic rocks display trace element characteristics typical of volcanic arc basalts, including enrichment in LIL and relative depletion in the HFS elements. Enrichments of Ce and Sm are a feature of calc-alkaline rocks, according to Pearce (1980) and also constitute geochemical evidence for sediment melting in subduction zones (Planck, 2005; Tollstrup and Gill, 2005). In the Zr - Ti/100 - Yx3 and Zr/4 - 2xNb - Y diagrams (Pearce and Cann, 1973; Meschede, 1986), almost all the rocks fall in the calc-alkaline and arc volcanic basalt fields (Fig. 8). The low Nb/Zr, Tb/Lu and Nb/La ratios (Fig. 9) are consistent with a N-MORB type source for all the these dyke rocks

(Kimura et al., 2002). The high Zr/Hf and La/Sm ratios in intermediate and acidic rocks reflect the role of some mantle minerals such as ilmenite and rutile controlling the melting process (Green, 1995). The Tb/Lu ratio (MREE/HREE) indicates that the liquids formed by decompressional melting of shallow mantle material in the spinel stability field as it rised during crustal thinning.

DISCUSSION

Dyke swarms are generally considered to be good markers for understanding the geological history. Dyke distribution and orientation contribute to elucidating tectonic processes active at the times of their emplacement (Hoek, 1991; Campbell and Sewell, 1997). They also provide geochemical indicators of magma sources that are useful for discussing their petrogenesis and supporting geotectonic models (Hamilton, 1977; El-Aouli et al., 2001; Melluso et al., 2001).

During Late Proterozoic times, the Anti-Atlas belt was the site of abundant volcanism dominated by acidic and intermediate rocks (andesite and rhyolite lavas and pyroclastic rocks) with calc-alkaline characters. These extrusive rocks are associated with high-K calc-alkaline intrusive rocks primarily in the Sirwa Massif and Ifni Inlier (El-Khanchaoui et al., 2001, Mortaji et al., 2005). One of the most common assumptions in igneous petrology is that all calc-alkaline series are related to a subduction environment. On the basis this assumption, the Upper Proterozoic calc-alkaline magmatism of the Anti-Atlas has been traditionally interpreted as a classic case of subduction-related volcanism (Bajja, 1987; Reguragui, 1997; Zahour et al., 1999). However, this interpretation is not universal (Doblas et al., 2002; Ikenne et al., 2004; Mortaji et al., 2005).

Recent investigations argue that the calc-alkaline signature is not automatically related to subduction and can be generated in a non-subduction environment. For example, Tertiary calc-alkaline magmatism of the Northwest Pacific is proposed to be driven by lithospheric extension and subsequent decompression melting of subcontinental lithospheric crust and mantle enriched by a previous subduction event (Hooper et al., 1995). Similarly, mafic volcanism in the Long Valley caldera area of eastern California follows a calc-alkaline evolutionary trend but is related to recent lithospheric extension and melting of older, metasomatized lithosphere (Cousens, 1996). On the basis of geochemical data, Márquez et al. (1999) interpreted the calc-alkaline features of Chichinautzin volcanism in the Mexican Volcanic Belt as a result of magma mixing between ocean island basalt-type mafic magmas and silicic, crust-derived melts during rifting. In the same way, trace and rare earth elements and isotopic data (Sr, Nd and O) allow Morris and Hooper (1997) and Morris et al. (2000) to conclude that Eocene calc-alkaline rocks of the Colville igneous complex (Washington State, USA) were produced by partial melting of mid-Proterozoic mid-crustal sources or by mixing between Proterozoic lower-crust melts and mantle derived magmas.

In the Imiter Inlier, geological data argue for the emplacement of late Proterozoic volcanic rocks during a NNW-SSE extensional event which evolved into a sinistral-extensional tectonic environment (Leistel and Qadrouci, 1991; Ouguir et al., 1994; Levresse, 2001). The

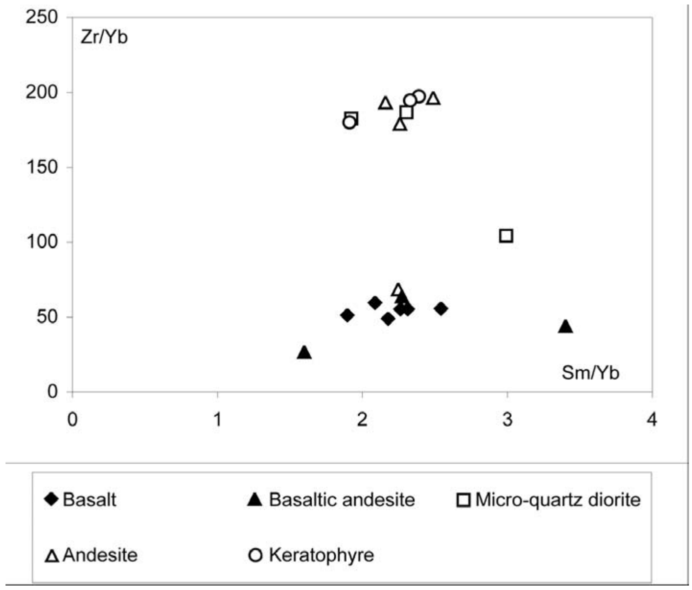

Fig. 5 - Zr/Yb *versus* Sm/Yb diagram showing distinction between mafic and acid and intermediate rocks.

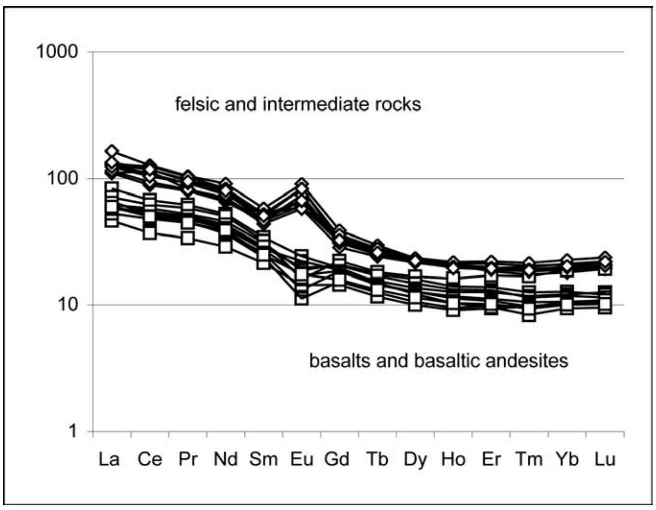

Fig. 6 - Chondrite-normalized (Evensen et al., 1978) REE patterns for the Imiter dyke rocks.

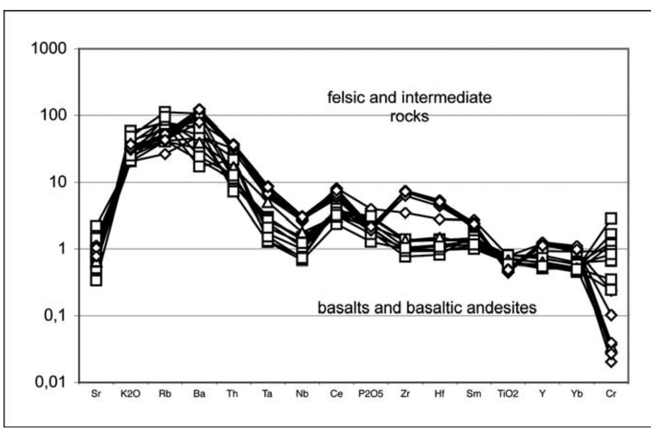

Fig. 7 - N-MORB-normalized (Pearce, 1980) multi-element diagram of the Imiter dyke rocks.

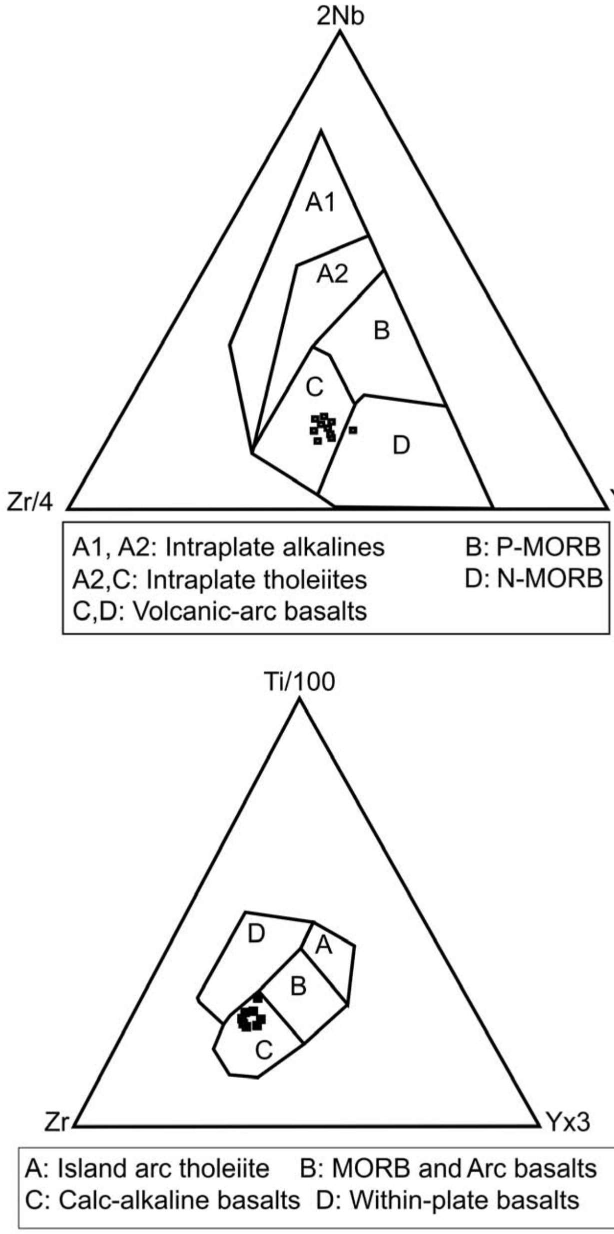

Fig. 8. - (a) Zr-Ti-Y Diagram (Pearce and Cann, 1973). (b) Zr-Nb-Y Diagram (Meschede, 1986).

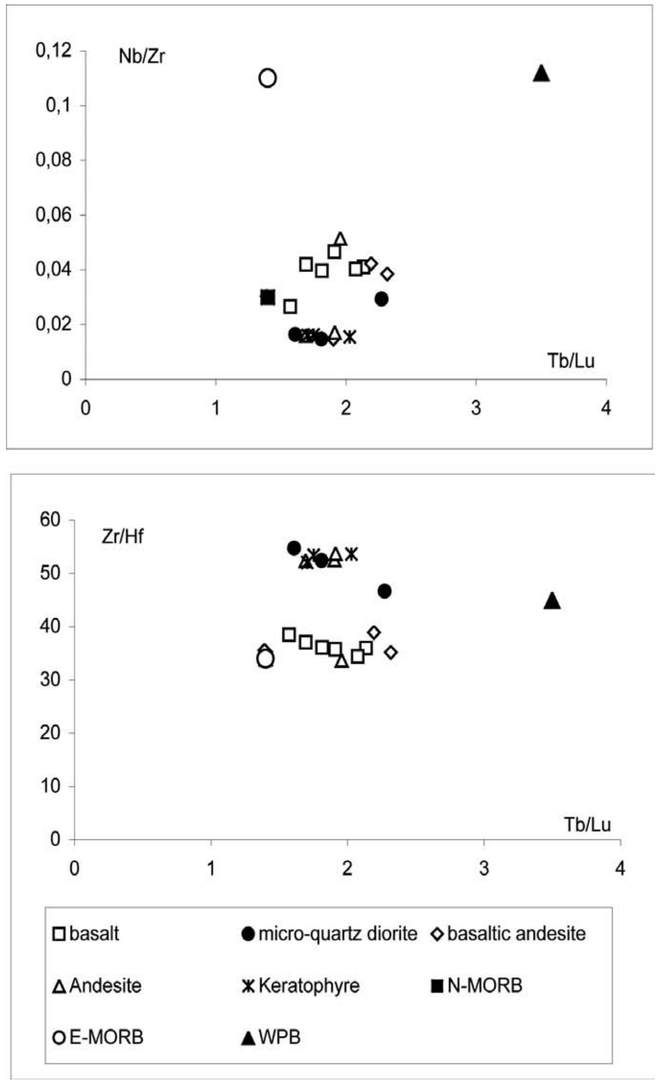

Fig. 9 - HFSE ratios vs Tb/Lu ratio for the Imiter dykes rocks. The Tb/Lu (MREE/HREE) ratio reflects the role of garnet in melt generation (Kimura et al., 2002).

dykes of the Imiter Inlier are related to the continuous rifting process that led to Paleozoic extension in the Anti-Atlas (Piqué et al., 1999; Belfoul et al., 2001; Benssaou and Hammoumi, 2001; Faik et al., 2001). The high-K calc-alkaline character of the dykes, emplaced in an extensional tectonic regime, is related to mantle melting in a post-collisional environment as suggested in similar cases from the Panafrican orogeny in the eastern border of the West African Craton (Liégeois et al., 1998) or in the South Carpathians (Duchesnes et al., 1998). The calc-alkaline signature can be related to: 1- subduction features in the mantle inherited from previous Proterozoic crustal sources; 2- presence of a preserved Panafrican subducted slab beneath this part of the Anti-Atlas (Leblanc and Lancelot 1980; Saquaque et al., 1989; Ennih and Liégeois, 2001), or 3- mixing of lower-crustal and mantle source magmas.

CONCLUDING REMARKS

Field and petrographic observations completed by geochemical data on dyke swarms of the Imiter Inlier allow us to suggest that:

1- The dyke rocks were emplaced within a E-W extensional stress field. Their spatial orientation, N-S to N70°E, appears to be controlled by pre-existing faults and stratification in host rocks;

2- The dykes played a significant role in the deposition of silver mineralization. The dykes acted as mechanical traps for the mineralization, either though their brittle structural behaviour or as a barrier to fluid flow;

3- The dykes were generated during a rift-related, decompressing melting event and their calc-alkaline geochemical features are not attributed to contemporaneous subduction.

ACKNOWLEDGEMENTS

This study was supported by the Ibn Zohr University of Agadir and The "Société métallurgique d'Imiter: SMI". We thank Sergio Rocchi and Giorgio Garuti for their critical comments and suggestions.

REFERENCES

Azizi Samir M.R, Ferrandini J. and Tane J.L., 1990. Tectonique et volcanisme tardi-Pan Africains (580-560 Ma) dans l'Anti-Atlas Central (Maroc): interprétation géodynamique à l'échelle du NW de l'Afrique. J. African Earth Sci., 10: 549-563

Bajja A., 1987. Nouvelles données pétrographiques et géochimiques sur les formations volcaniques précambriennes du Jbel Saghro (Anti-Atlas Marocain). Basaltes en coussin du PII et volcanites de la série de Ouarzazate PIII. PhD thesis, H.P. Univ., Nancy, 255 pp.

Baroudi Z., Beraaouz EH., Rahimi A.M., Saquaque A and Chouhaidi M.Y., 1999. Minéralisations polymétalliques argentifères d'Imiter (Jbel Saghro, Anti-Atlas, Maroc): Minéralogie, évolution des fluides minéralisateurs et mécanismes de dépôt. Chron. Rech. Min., 536-537: 91-112

Belfoul M.A., Faik F. and Hassenforder B., 2001. Evidence of a tangential tectonic event prior to the major folding in the Variscan belt of the western Anti-Atlas, Morocco. J. African Earth Sci., 32: 723-739.

Benssaou M. and Hamoumi N., 2001. L'Anti-Atlas occidental du Maroc: étude sédimentologique et reconstitutions paléogéographiques au Cambrien inférieur. J. African Earth Sci., 32: 351-372.

Campbell S.D.G. and Sewell R.J., 1997. Structural control and tectonic setting of Mesozoic volcanism in Hong Kong. J. Geol. Soc., 154: 1039-1052.

Cheilletz A., Levresse G., Gasquet D., Azizi Samir M.R., Zyadi R. and Archibald D.A., 2002. The Imiter epithermal deposit (Morocco): new petrographic, microtectonic and geochronological data. Importance of the Precambrian-Cambrian Transition for major precious metals deposits in the Anti-Atlas. Mineral. Dep., 37: 772-781.

Cousens B.L., 1996. Magmatic evolution of Quaternary mafic magmas at Long Valley Caldera and the Devils Postpile, California: Effects of crustal contamination on lithospheric mantle-derived magmas, J. Geophys. Res., 101: 27673-27689.

Doblas M., López-Ruiz J., Cebriá J-M., Youbi N. and Degroote E., 2002. Mantle insulation beneath the West African craton during the Precambrian-Cambrian transition. Geology, 30: 839-842.

Duchesne J.C., Berza T., Liégeois J.P. and Vander Auwera J. 1998. Shoshonitic liquid line of descent from diorite to granite: the late Precambrian post-collisional Tismana pluton (South Carpathians, Romania). Lithos, 45: 281-303.

Ducrot J. and Lancelot J.R., 1977. Problème de la limite Précambrien-Cambrien. Étude radiochronologique par la méthode U-Pb sur zircons du volcan du jbel Boho (Anti-Atlas marocain). Can. J. Earth Sci., 14: 2771-2777.

El-Aouli E.H., Gasquet D. and Ikenne M., 2001. Le magmatisme basique de la boutonnière d'Igherm (Anti-Atlas occidental, Maroc): un jalon des distensions néoprotérozoïques sur la bordure nord du craton ouest-africain. Bull. Soc. Géol. France, 172: 309-317.

El-Khanchaoui T. Lahmam M. El-Boukhari A. and Beraaouz E-H., 2001. Neoproterozoic granitoids from Khzama, central Anti-Atlas, Morocco: evolution markers from arc magmatism to alkaline magmatism, J. African Earth Sci., 32: 655-676.

Ennih N. and Lièegeois, J.P., 2001. The Moroccan Anti-Atlas: the West African craton passive margin with limited Pan-African activity. Implications for the northern limit of the craton. Precamb. Res., 112: 289-302.

Evensen N.H., Hamilton P.J. and O'Nions R.K., 1978. Rare earth abundances in chondrite meteorites. Geochim. Cosmochim. Acta, 42: 1199-1212.

Faik F., Belfoul M-A., Bouabdelli M. and Hassenforder B., 2001. The structures of the Late Neoproterozoic and Early Palaeozoic cover of the Tata area, western Anti-Atlas, Morocco: polyphased deformation or basement/cover interactions during the Variscan orogeny? J. African Earth Sci., 32: 765-776.

Gasquet D., Chevremont P., Baudin T., Chalot-Prat F., Guerrot C., Cocherie A., Roger J., Hassenforder B.Y. and Cheilletz A., 2004. Polycyclic magmatism in the Tagragra d'Akka and Kerdous-Tafeltast inliers (Western Anti-Atlas, Morocco). J. African Earth Sci., 39: 267-275.

Gasquet D., Levresse G., Cheilletz A., Azizi-Samir M.-R and Mouttaqi A., 2005. Contribution to a geodynamic reconstruction of the Anti-Atlas (Morocco) during Pan-African times with the emphasis on inversion tectonics and metallogenic activity at the Precambrian-Cambrian transition. Precamb. Res., 140: 157-182.

Green T.H., 1995. Significance of Nb/Ta as an indicator of geochemical processes in the crust-mantle system. Chem. Geol., 120: 347-359.

Guillou J.J., Monthel J., Samama J.C and Tijani A., 1988. Morphologie et chronologie relative des associations minérales di gisement mercuro-argentifère d'Imiter (Anti-Atlas- Maroc). Notes Mém. Serv. Géol. Maroc, 44: 215-228.

Hamilton J.O., 1977. Sr isotope and trace element studies of the Great Dyke and Bushveld mafic phase and their relation to Early Proterozoic magma genesis in Southern Africa. J. Petrol., 18: 24-52.

Hassenforder B., 1987. La tectonique panafricaine et varisque de l'Anti-Atlas dans le massif de Kerdous (Maroc). Thèse Doct.Es-sci. Univ. L. Pasteur, Strasbourg, 249 pp.

Hoek J.D., 1991. A classification of dyke-fracture geometry with examples from Precambrian dyke swarms in the Vestfold Hills, Antarctica. Geol. Rundsch., 80: 233-248.

Hooper P.R., Bailey D.G. and Mccaley Holder G.A., 1995. Tertiary calc-alkaline magmatism associated with litospheric extension in the Pacific Northwest. J. Geophys. Res. 100: 10,303-10,319.

Ikenne M., Ennaciri A., Ouguir H., Zyadi R. and Mouhajir M., 2004. The dyke swarm of the Neoproterozoic Imiter inlier Anti-Atlas Morocco): geotectonic setting and relationship to silver mineratizations. IGCP Symp. Craton and metacratons and bounding orogens west African craton and mobil belts. December 2004, Noukchott, Abstr., p. 69.

Kimura J., Manton W.I., Sun C, Iizumi S, Yoshida T. and Stern R.J., 2002. Chemical diversity of the Ueno Basalts, Central Japan: Identification of mantle and crustal contributions to arc basalts. J. Petrol., 43: 1923-1946.

Leblanc M., 1981. Ophiolites precambriennes et gites arsenides de cobalt (Bou Azzer, Maroc). Notes Mém. Serv. Géol. Maroc, 280, 306 pp.

Leblanc M and Lancelot J.-R., 1980. Interprétation géodynamique du domaine panafricain (Précambrien terminal) dans l'Anti-Atlas (Maroc) à partir de données géologiques et géochronologiques. Can. J. Earth Sci., 17: 142-155.

Leistel J.-M. and Qadrouci A., 1991. Le gisement argentifère d'Imiter (Protérozoïque supérieur de l'Anti-Atlas, Maroc). Contrôles des minéralisations, hypothèses génétiques et perspectives pour l'exploration. Chron. Rech. Min., 502: 5-22.

Levresse G., 2001. Contribution à l'établissement d'un modèle génétique des gisements d'Imiter (Ag-Hg) Bou Madine (Pb-Zn-Cu-Au) et Bou Azzer (Co-Ni-As-Au-Ag) dans l'Anti-Atlas Marocain. PhD thesis, INPL, Nancy, 191pp.

Levresse L., Cheilletz A., Gasquet D., Reisberg L., Deloule E., Marty B. and Kyser K., 2004. Osmium, sulphur, and helium isotopic results from the giant Neoproterozoic epithermal Imiter silver deposit, Morocco: evidence for a mantle source. Chem. Geol., 207: 59-79.

Liégeois J.P., Navez J., Hertogen J. and Black R. 1998. Contrasting origin of post-collisional high-K calc-alkaline and shoshonitic versus alkaline and peralkaline granitoids. The use of sliding normalization. Lithos 45: 1-28.

Maacha L, Azizi-Samir M.-R and Bouchta R., 1998. Gisement cobaltifère de BouAzzer (Anti-Atlas) structure, minéralogie et conditions de genèse. Chron. Rech. Min., 531-532: 65-75.

Marini F. and Ouguir H., 1990. Un nouveau jalon dans l'histoire de la distension pré-panafricaine au Maroc: Le Précambrien II des boutonnières du Jbel Saghro nord-oriental (Anti-Atlas, Maroc). C.R. Acad. Sci., Paris, 310: 577-582.

Márquez A., Oyarzun R., Doblas M. and Verma S.P., 1999. Alkalic (OIB-type) and calc-alkalic volcanism in the Mexican volcanic belt: a case for plume-related magmatism and propagating rifting at an active margin? Geology, 27: 51-54.

Melluso L., Morra V., Brotzu P. and Mahoney J.J., 2001. The Cretaceous igneous province of Madagascar: geochemistry and petrogenesis of lavas and dykes from the central-western sector. J. Petrol., 42: 1249-1278.

Meschede M., 1986. A method of discriminating between different types of mid-ocean ridge basalts and continental tholeiites with the Nb-Zr-Y diagram. Chem. Geol., 56: 207-18.

Morris G.A., and Hooper P.R., 1997. Petrogenesis of the Colville igneous complex, northeast Washington: Implications for Eocene tectonics in the northern U.S. Cordillera. Geology, 25: 831-834.

Morris G.A., Larson P.B. and. Hooper P.R., 2000. 'Subduction Style' magmatism in a non-subduction setting: the Colville Igneous Complex, NE Washington State, USA. J. Petrol., 41: 43-67.

Mortaji A., Gasquet D., Ikenne M., Barbey P., Beraaouz E-H. and El-Aouli E-H., 2005. Les granitoïdes de la boutonnière d'Ifni dans le cadre de l'évolution panafricaine de l'Anti-Atlas (Anti-Atlas occidental - Maroc). In: 4th 3MA Coll., Agadir. Abstr., p. 13.

Oudra M., Beraaouz E.-H., Ikenne M., Gasquet D. and Soulaimani A., 2005. la tectonique panafricaine du secteur d'Igherm: implication des dômes extensifs tardi-orogéniques (Anti-atlas Occidental, Maroc). Estud. Geol., 61: 177-189.

Ouguir H., Macaudiere J., Dagallier G., Qadrouci A.-Y. and Leistel J.M., 1994. Cadre structural du gîte Ag-Mg d'Imiter (Anti-Atlas, Maroc), implications métallogénique. Bull. Soc. Géol. France, 165: 233-248.

Pearce J.A., 1980. Geochemical evidence of the genesis and eruptive setting of lavas from Tethyan ophiolites. In: A. Panayiton (Ed.), Ophiolites, Proceed. Intern. Ophiolites Symp. Cyprus, p. 261-272.

Pearce J.A. and Cann J.R., 1973. Tectonic setting of basic volcanic rocks determined using trace element analyses. Earth Planet. Sci. Lett., 19: 290-300.

Piqué A., Bouabdelli M., Soulaimani A., Youbi N. and Iliani M., 1999. Les conglomérats du PIII (Néoprotérozoïque supérieur) de l'Anti-Atlas (Sud du Maroc): molasses panafricaines, ou marqueurs d'un rifting fini-Protérozoïque? C.R. Acad. Sci. Paris, Sci. Terre Planètes, 328: 409-414.

Planck T., 2005. Constraints from Thorium/Lanthanum on sediment recycling at subduction zones and the evolution of the continents. J. Petrol., 46: 921-944.

Reguragui M., 1997. Les formation volcano-sédimentaire et le magmatisme orogénique et anorogénique du néoprotérozoïque supérieur et terminal d'Askaoun (Sirona Occidental, Anti Atlas Central Maroc) Pétrologie, Géochimie et Typologie des zircons. PhD Thesis, Univ. Cadi Ayyad, Marrakech.

Saquaque A., Admou H., Karson S., Hefferan K. and Reuber I., 1989. Precambrian accretionary tectonics in the Bou-Azzer-El Graara region, Anti-Atlas, Morocco. Geology, 17: 1107-1110.

Soulaimani A, Bouabdelli M. and Piqué A., 2003. The Upper Neoproterozoic-Lower Cambrian continental extension in the Anti-Atlas (Morocco). Bull. Soc. Géol. France, 174: 83-92.

Soulaimani A. and Pique A., 2004. The Tasrirt structure (Kerdous inlier, Wesren Anti-Atlas, Morocco): a late Pan-African transtensive dome. J. African Earth Sci., 39: 247-255.

Thomas R.J., Chevakier L.P., Gresse P.G., Harmer R.E., Eglington B.M., Armstrong R.A., De Beer C.H., Martini J.E.J., De Kock G.S., Macey P.H. and Ingram B.A., 2002. Precambrian evolution of the Sirwa Window, Anti-Atlas Orogen, Morocco. Precamb. Res., 118: 1-57.

Thomas R.J., Fekkak A., Ennih N., Errami E., Loughlin S.C., Gresse P.G., Chevakier L.P. and Liegeois J.P. 2004. A new lithostratigraphic framwork for the Anti-Atlas Orogen, Morocco. J. African Earth Sci., 39: 217-226.

Tollstrup D.L. and Gill J.B., 2005. Hafnium systematics of the Mariana arc: Evidence for sediment melt and residual phases. Geology, 33: 737-740.

Walsh G.J., Aleinikoff J.N., Benziane F., Yazidi A. and Armstrong T.R., 2002. U-Pb zircon geochronology of the Paleoproterozoic Tagragra de Tata inlier and its Neoproterzoic cover, western Anti-Atlas, Morocco. Precamb. Res., 117: 1-20.

Zahour G., El-Khanchaoui T., Chabane A., Youbi N. and El-Boukhari A., 1999. Les ignimbrites asssociées aux volcanites Néoprotérozoïque du terminal de la boutonnière de Siroua (Anti-Atlas central, Maroc): relation génétique et environnement géotectonique, Africa Geosci. Rev., 6: 177-198.

Received, March 3, 2007
Accepted, November 29, 2007